Chinese Journal of Electronics
Vol.XX, No.X, Jan. 20XX

Visual Exploration of Differences among DTI Fiber Models*

Mei Honghui[1], CHEN Haidong[1] , GUO Fangzhou[1] , ZHANG Fan[2] , SONG Zhang[3] , WANG Guizhen[1] and CHEN Wei[1]

(1. *State Key Lab of CAD&CG, Zhejiang University, China*)

(2. *Zhejiang University of Technology, China*)

(3. *Computer Science and Engineering, Mississippi State University, US*)

Abstract — In-vivo studies of fibrous structures require non-invasive tools, of which one is fiber tracking based on Diffusion Tensor Imaging (DTI) datasets. Different fiber models can be produced from different DTI images, which may vary from subject to subject due to variations in anatomy, motions in scanning, and signal noises. Additionally, parameters of the tracking method also have a great influence on resulting models. Illustrating, exploring, and analyzing differences among DTI fiber models are crucial for the purposes of group comparison, atlas construction, and uncertainty analysis. Conventional approaches illustrate fiber models in 3D space and explore differences either voxel-wisely or fiber-based. However, these approaches rely on accurate alignment processes and may easily be disturbed by visual clutters. In this paper, we introduce a two-phase projection technique to illustrate a complex 3D fiber model with a unique 2D map to characterize features for further exploration and analysis. Moreover, regions of significant differences among the maps are marked out. In these 2D maps, differences can be easily distinguished without occlusions that often occur in 3D spaces. To facilitate comparative analysis from multiple perspectives, we design an interface for interactive exploration. The effectiveness of our approach is evaluated with two datasets.

Key words — Diffusion Tensor Imaging, fiber tracking, difference visualization, visual exploration.

I. Introduction

Diffusion Tensor Imaging (DTI) [1] is a non-invasive *in vivo* magnetic resonance imaging technique that measures the diffusion of water in biological tissues. In tissues containing fibrous structures such as the brain white matter, the diffusion is fast along the fibers and slow in the directions perpendicular to the fibers [2]. By fitting the distribution of water molecules with a Gaussian model and representing this Gaussian model as a second-order tensor, a DTI tensor volume can be reconstructed from the raw Diffusion Weighted Imaging (DWI) volumes [3]. Tracing paths through the entire tensor volume produces a collection of DTI fibers, i.e., a DTI fiber model. This process is known as fiber tractography or fiber tracking [4], which has been proven to be a useful technique for analyzing anatomical connectivity.

In spite of its potential, DTI remains limited in applications. Uncertainty is a major reason. DTI fibers vary from subject to subject due to variations in anatomy, and from scan to scan because of different subject positions, scanning motions and noises [2]. They are also sensitive to various parameters in tractography such as the integration step size and stopping criteria (e.g., the stopping anisotropy thresholds) [5]. Statistical and probabilistic techniques (e.g., Wild Bootstrap [6] and stochastic tracking based on a Bayesian framework [7]) are commonly used to capture and quantify these uncertainties.

Comparatively visualizing and analyzing different DTI datasets can help users identify the differences and understand the uncertainty. To achieve this, one of the major task is to represent and visualize differences within a collection of DTI datasets. Direct comparison of 3D DWI or DTI volumes [8, 9] demands an accurate alignment process and misses the anatomical connectivity within each volume. Explicit depiction of the geometrical differences among DTI fiber models in the 3D space [5, 10] is hindered by the spatial complexity of dense fibers. Comparison by using statistical tractography metrics [11] such as the average fiber length lacks the ability to locate regions of differences.

*Manuscript Received June XX, 20XX; Accepted July XX, 20XX. This work is supported by the National Natural Science Foundation of China (No.XXXX, No.XXXX).

 DOI:10.1049/cje.20XX.0X.0XX

Projection techniques have been widely used to construct a visual representation of a high-dimensional dataset in a way that the low dimensional layout respects the proximities among instances in the source dataset [12]. They provide a holistic view of the overall structures and distributional patterns under the given views. Successful applications in visualization include document exploration [13], data organization [14], and subspace exploration [15]. Recent work extends this scheme into the exploration of DTI fiber models [16, 17]. However, these solutions are well designed to explore the content of a single fiber model and cannot be directly employed to analyze multiple fiber models. The main reason is that different fiber models do not share a common space for projection and comparison.

In this paper, we present a comparative visualization approach that supports quick identification and intuitive exploration of differences among DTI fiber models. After all datasets are registered into a common coordinate space, fiber models are embedded on a 2D visual plane by means of a two-phase projection technique. The embedding of a fiber model constructs a 2D scatterplot which are further represented as a continuous density map and a contoured density map. To provide an overview of the major differences among these maps, regions of differences (RoDs) are computed with a simple flood fill algorithm. Both *Juxtaposition* and *Explicit Encoding* are utilized within the visual exploration interface. We have verified the effectiveness of our approach on several DTI datasets.

In summary, the contributions of this paper are:

- A novel low-dimensional representation of complex fiber models for visual comparison and further regions of differences identification;
- An integrated visualization interface that provides users an intuitive way to explore differences in multiple perspectives.

The remaining parts are organized as follows. Related work are summarized in Section II. Our approach is elaborated in Section III. The visual exploration interface is described in Section IV. The implementation details are presented in Section V. The results of our approach are discussed in Section VI. Finally, we conclude this paper in Section VII.

II. Related Work

Our work is related to several topics of visualization research including comparative visualization, uncertainty visualization, and DTI fiber model exploration.

1. Comparative Visualization Recently, a wide variety of approaches have been developed in the field of comparative visualization. Gleicher et al. [18] presented a general taxonomy of visual designs for comparisons and summarized these designs into three categories: *Juxtaposition*, *Superposition*, and *Explicit Encoding*. Zhou et al. [19] outlined a group of comparison metrics for quantifying the difference between a visualization of a computer simulation and a photographic image. Verma and Pang [20] proposed several solutions for comparative flow visualization at image level, data level, and feature level. Malik et al. [21] introduced a novel multi-view design for comparing and visualizing gray values and edges of several 3D CT datasets simultaneously. They first divide the plane into hexagonal regions and then subdivide each region into multiple sectors to depict details from different datasets. This design allows users to identify difference very easily but is limited to the number of datasets. Schmidt et al. [22] proposed an approach for comparative visualization of multiple images. Their technique overcomes the scalability issues pertaining to the number of objects for comparison, and allows users to perform detailed cluster analysis in the regions of significant differences. Oelke et al. [23] designed a glyph representation called topic coins to encode information necessary for comparative document analysis. Piringer et al. [24] developed an interactive approach for comparative visual analysis of 2D function ensembles. Our approach employs both the *Juxtaposition* and *Explicit Encoding* design to identify and study differences among DTI fiber models.

In the field of DTI study, comparison is an important means to locate changes related to development, degeneration, and disease. One pioneering work [10] compares the generated fibers in the 3D space and uses saturation to indicate the magnitude of differences between corresponding points. This method is simple and intuitive, but only focuses on fiber structures and may result in visual clutter. In order to investigate the diffusion properties along fibers, group statistical analysis [25, 26] is performed after aligning datasets and representing fibers with continuous functions. The key idea behind this method is that fibers are represented with a simplified form (like B-spline) to facilitate statistical comparison.

To study the diffusion property volumes such as the Fractional Anisotropy (FA) for multiple subjects, Smith et al. [9] presented Tract-Based Spatical Statistics (TBSS), which is a voxel wise analysis framework via a nonlinear registration followed by projection onto a skeleton. Nevertheless connectivity information is ignored by this method. In addition to the study on DTI volumes, there has been some work on general-purpose group analysis of geometrical or volumetric datasets. For instance, Elvins et al. [27] proposed to use a density histogram to describe a volume dataset. Though simple, it provides very low discrimination power. Other different feature descriptors have been proposed to accomplish similarity assessment,

including transformational [28], topological [29], and statistical [30] signatures. Different from these methods, our approach generates a unique 2D signature map of a 3D fiber model for further comparison and exploration.

2. Uncertainty Visualization Analyzing and visualizing the differences among datasets play a central role for studying uncertainty. General techniques adopt visual variables [31, 32], glyphs [33, 34], and animations [35] to depict uncertainty. In the context of DTI study uncertainty arises from multiple aspects such as noise, motions, variations in anatomy, and parameters in fiber tracking. Uncertainty quantification usually targets the characteristics of the diffusion tensors including the main direction and fractional anisotropy. Friman et al. [7] employed a Bayesian framework to model the uncertainty associated with fiber paths. Chung et al. [36] exploited the non-parametric statistical technique Bootstrap to quantify uncertainties of diffusion tensor parameters. Later the Wild Bootstrap approach [6] that requires only one acquisition of DWIs while achieving similar effects as the standard Bootstrap methods was used to measure uncertainty. Brecheisen et al. [5] designed a visualization tool to interactively study the influence of stopping criteria on fiber tracking. To show the shape uncertainty in fiber tracking, illustrative visualization methods were exploited to explicitly depict uncertainties in the 3D fiber space [37].

3. DTI Fiber Model Exploration Exploring and manipulating a DTI fiber model in the 3D space pose many challenges, especially on providing intuitive interaction. Embedding the fibers into a 2D space with projection techniques has been demonstrated to be an effective means to study fiber models. Chen et al. [16] designed a novel interface by utilizing the multidimensional scaling (MDS) technique to facilitate quick and accurate 3D fiber selection on a 2D plane. Similarly, Jianu et al. [38] introduced a visual exploration paradigm by embedding 3D fibers on a 2D plane to reduce navigation efforts. Poco et al. [17] exploited the *Local Affine Multidimensional Projection (LAMP)* [39] technique to support fast visual exploration of large collection of DTI fibers. Demiralp et al. [40] presented a 2D path representations with a planar projection technique for studying fiber dataset. A web interface was also designed to support exploration. In general, the 2D visual representation captures the structures and patterns of the source dataset and is free of occlusion during interaction and exploration. However, most of these approaches focus on single fiber model exploration. This paper advances a computation-efficient two-phase projection technique to compare multiple fiber models.

III. Our Approach

Fig. 1 shows a schematic overview of our approach. In general, our approach consists of three main components. The preprocessing component registers all DTI volumes into a common space and reconstructs a 2nd order tensor in each voxel based on the Gaussian diffusion model. Fibers are then extracted according to the user-defined tracking parameters. Instead of direct comparing fiber models in the 3D space, we employ a two-phase projection technique followed by the density estimation to reformulate each fiber model as a 2D signature map. As a key benefit, these maps allow for intuitive recognition and quick comparison. A number of views and interactions are provided to discover and study differences among fiber models.

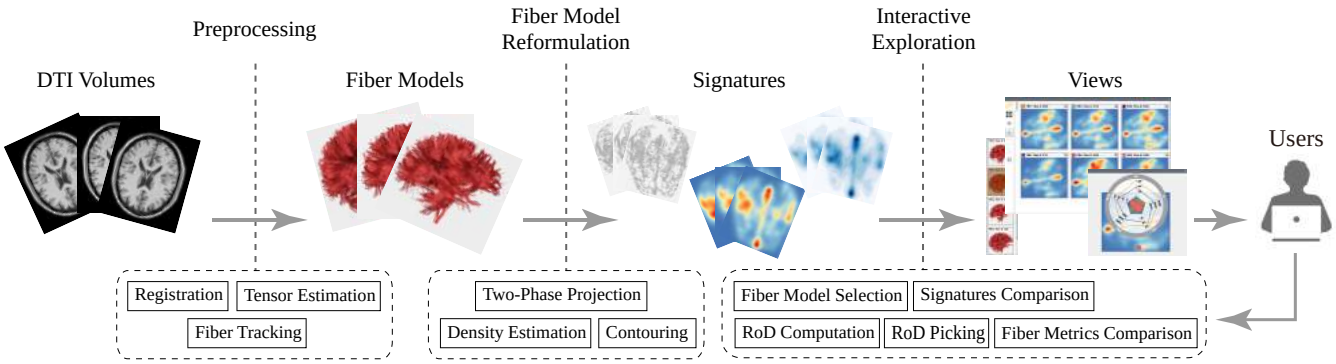

Fig. 1. An overview of our difference computation, visualization, and exploration pipeline for DTI fiber models.

1. Preprocessing

Typically a DTI volume dataset has at least six 3D diffusion weighted images that record the diffusion strength in various directions and at least one 3D image with no diffusion [9]. Due to variations in scanning devices and positions, different datasets usually do not share the same coordinate space. For accurate comparison, the alignment of all datasets to a target is required. In our approach, FLIRT [41] is employed to perform a rigid registration on all b_0 images (i.e. the no-diffusion images).

After registration, a diffusion tensor field can be reconstructed of a DTI dataset, using the least square fitting method. By tracing paths with numerical integration methods such as the second-order Runge-Kutta (RK2), a fiber model that captures the connectivity information of a DTI dataset is produced.

2. Fiber Model Reformulation

Let $\Gamma = F_1 \cup F_2 \cup ... \cup F_N$ be a fiber corpus consisting of N fiber models, and fiber model $F_i = \{f_i^j, j = 1, 2, ..., N_i\}$ has N_i fibers, where f_i^j denotes a fiber. To represent the variations among different fiber models, our approach generates a unique signature map S_i for each fiber model F_i.

Directly representing each fiber model F_i in the 3D space may cause visual clutter. Projection techniques [16, 17] that focus on building a 2D visual representation for a fiber model can alleviate this issue. Before projection, all fibers must be reparameterized to make sure that they have the same number of vertices and orientations in order to calculate similarity measure used in LAMP technique [39, 17].

To embed fibers on the visual plane, our approach employs the *Landmark MDS (LMDS)* technique [42] which performs a two-phase projection.

Phase 1 A subset of fibers $\Gamma_{landmark} \subset \Gamma$, namely the *landmark fibers*, are selected from the fiber corpus. These fibers are then projected to the 2D visual plane with the accurate classic MDS technique, yielding a 2D embedding L. Each column of the matrix L is a 2D location corresponding to a fiber.

Phase 2 The 2D location l_r of a fiber $r \in F_i$ on the visual plane is then computed by an affine linear transformation [42] according to its squared distances to the landmark fibers.

$$l_r = -\frac{1}{2} L^{\dagger^T} (\vec{\delta_r} - \vec{\delta_\mu}), \tag{1}$$

where $L^{\dagger^T}$ represents the pseudo-inverse transpose of L, the vector $\vec{\delta_r}$ contains the squared distances between fiber r to all landmark fibers, and $\vec{\delta_\mu}$ is the mean vector of the pairwise squared distance matrix for landmark fibers.

Throughout this paper, the longer mean of thresholded closest distance [43] is used to measure the dissimilarity between fibers:

$$d(p, q, t) = max(d_t(p, q, t), d_t(q, p, t)), \tag{2}$$

where $d_t(p, q, t) = mean_{u \in p, (min_{v \in q} \| u - v \| > t)} min_{v \in q} \| u - v \|$, u and v are vertices of fiber p and q respectively. The minimum threshold t is set to 0.5mm as suggested by [43].

Compared with other methods, this projection scheme reduces the computational complexity of dissimilarity estimation from $O(n^2)$ to $O(m^2 + m \times n)$. $m = |\Gamma_{landmark}|$ is the number of landmark fibers. $n = |\Gamma|$ is the number of fibers in the fiber corpus. In practice, the algorithm works well when m is set to $\sqrt{n}$. One additional benefit of this scheme is its intrinsic parallelizability, because each fiber is embedded independently from each other using a fixed linear transformation.

In our implementation, we randomly select landmark fibers as random selection produces similar results to those use optimized selection methods provided in [42].

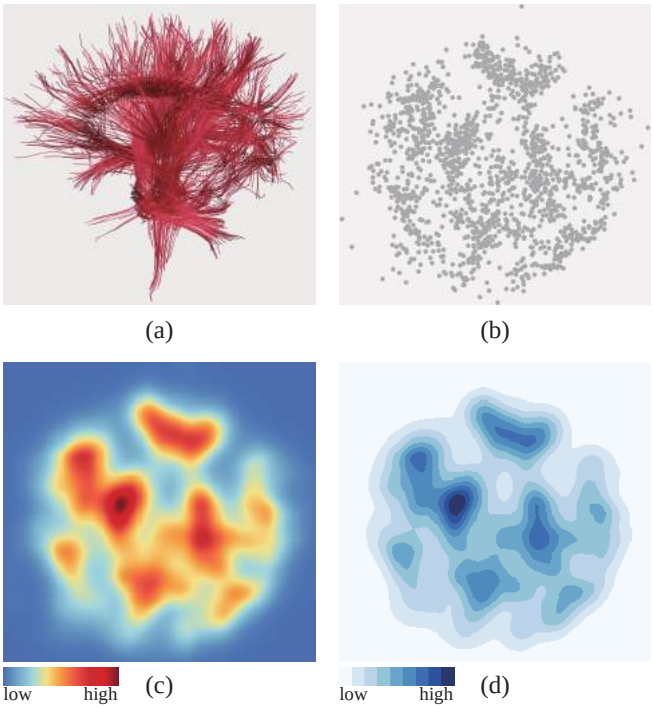

Fig. 2. The signature of a fiber model (a) consisting of 1622 fibers. (b) The 2D embedding shown as a scatterplot. (c) The continuous density map. (d) The contoured density map.

3. Density Estimation

The embedding of each fiber model F_i yields a 2D scatterplot (see Fig. 2 (b)). Similar fibers are positioned close to each other in this scatterplot. To facilitate recognition and visualization, we further apply the kernel density estimation (KDE) to the scatterplot to produce a continuous 2D density map D_i (see Fig. 2 (c)).

$$D_i(x) = \sum_{r \in F_i} K_h(x - l_r), \tag{3}$$

where l_r denotes the 2D location of fiber r, $K_h(\cdot)$ is a kernel function with bandwidth h which determines the smoothing degree of the reconstructed density field. Different from the conventional KDE method, we do not use the fiber count N_i to normalize density for the purpose of directly comparing densities at a location x. A Gaussian kernel is used in our approach with the bandwidth h determined by the Silverman's rule of thumb [44] and can be modified by the user.

By dividing the range of the computed density into multiple intervals and coloring the elements within each interval, another contour-like map (see Fig. 2 (d)) is generated. The contoured density map can be deemed as an abstraction of the continuous density map. It suppresses many undesired details for a quick comparison.

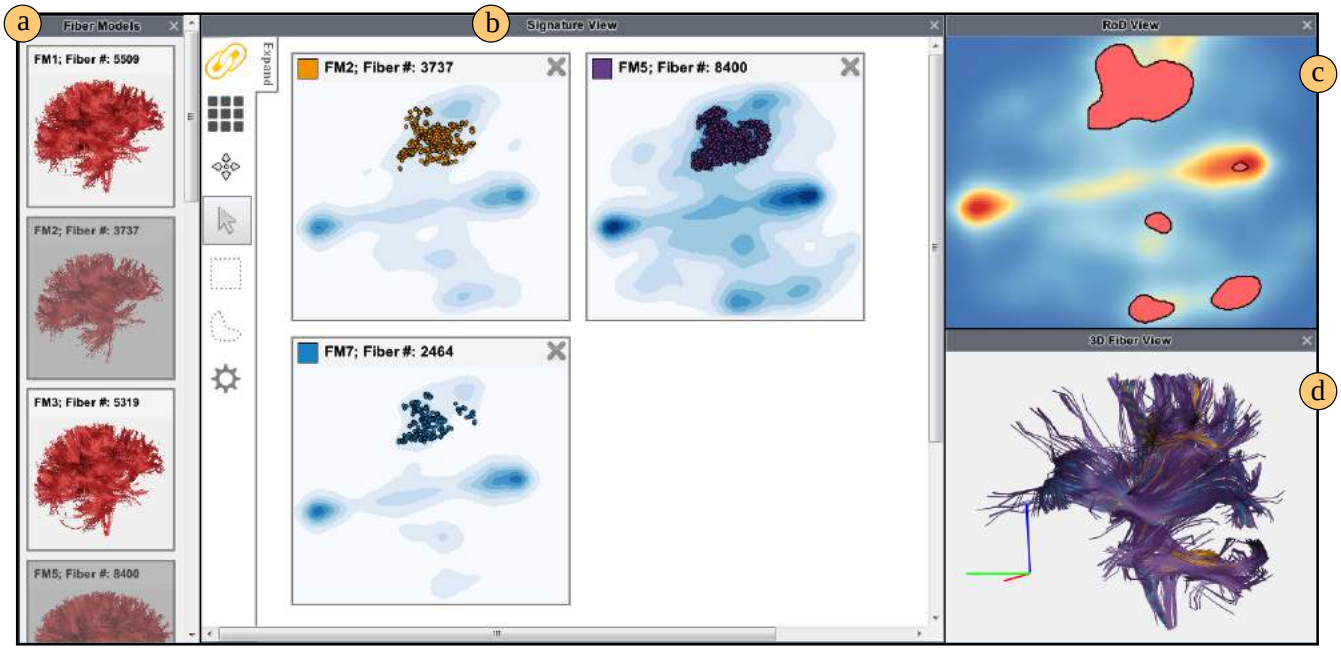

Fig. 3. The main views of our visual exploration interface. (a) The fiber model list view. (b) The signature view. (c) The RoD view. (d) The 3D fiber view.

Consequently, each fiber model uniquely determines a signature map S_i: a discrete scatterplot associated with a continuous density map and a contoured density map.

4. Region of Difference Estimation

The *Juxtaposition* design that displays visualizations side by side in multiple views is a common way to explore differences and similarities among multiple datasets. However, it requires a large amount of mental workload to identify the differences. Inspired by [22], we employ an explicit difference encoding to assist users in identifying regions of differences (RoDs).

Specifically, the density variance $V(x)$ at each location x is computed as:

$$V(x) = \frac{1}{N}\sum_{i=1}^{N}(D_i(x) - \mu(x))^2, \tag{4}$$

where $\mu(x)$ is the average density at location x. In our implementation, we compute the density variance for each pixel of the densities generated by KDE. Then, a user-adjustable threshold is used to filter out pixels of low density variations. At last, the region growing algorithm [22] is employed to group disjoint pixels into regions. The resultant RoDs provide an overview of differences residing in the shown signatures. Users can flexibly pick a RoD to further explore the statistical differences of fibers embedded into this region.

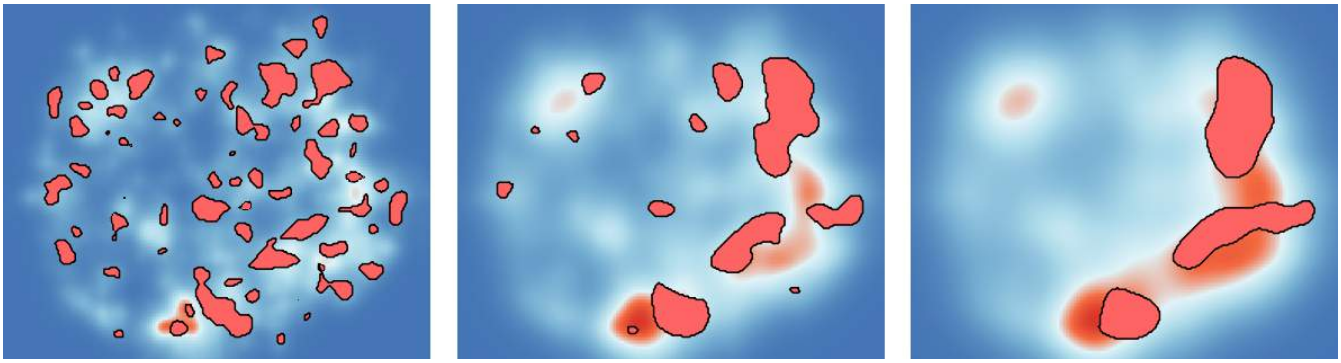

Fig. 4. Calculated RoDs when using different bandwidth h in density estimation. h increases from left to right.

As RoDs are generated from the results of density estimation, they are affected by the bandwidth h of the kernel function. When bandwidth increased, number of RoDs will be reduced and adjacent RoDs tend to merge together (Fig.4).

IV. Visual Exploration Interface

The fiber models, the generated signatures, and the computed RoDs can be interactively explored in our integrated interface composed of a set of linked views. Fig. 3 illustrates an overview of this interface. Please refer to the supplementary video for more demonstrations.

1. Fiber Model List View

To help users gain an overview of each fiber model, we design the fiber model list view that takes a small multiple visual form. Each fiber model is represented as a rectangular glyph. Basic information including the name, the fiber count, and a snapshot are embedded (see Fig. 3 (a)). By double clicking the glyph, a widget is popped up to explore the fiber model in a 3D view. The fiber models of interest can be dragged to the signature view for further exploration and comparison. The selected fiber models are highlighted with a grey mask.

2. Signature View

Instead of comparing fiber models in the 3D space, users can compare the signatures in the signature view to discover differences and similarities among fiber models. The signature view employs a juxtapositional design which shows the selected fiber models' signatures in a side-by-side fashion. Though limited capability is provided in this view to help users quickly identify regions of significant differences, it does allow for exploring each single fiber model with others as a context. Basic information such as the fiber count is embedded as well. Users can remove a signature from this view. In addition, following interactions are supported:

Switching Users can choose different forms of signatures (including the discrete scatterplot, the continuous density map, and the contoured density map) to be displayed.

Dragging To facilitate comparison, signatures of interest can be dragged close to each other.

Selection Two types of intuitive selection tools are provided to specify a region of interest in the discrete scatterplot. The *box* selection tool is used to specify a rectangular region. The *lasso* selection tool allows for drawing an arbitrary shaped region. Linked selection is also implemented to simultaneously specify identical regions on different signatures. The selected fibers are immediately shown in the 3D fiber view.

3. RoD View

As described above, the signature view shows the details of the selected fiber models' signatures. It is of equal, if not more, importance to offer an overview of major differences among these signatures. For this purpose, we design the RoD view. The identified RoDs are rendered as polygons overlaid on the average density map (see Fig. 3 (c)). The Focus+Context interaction is implemented to inspect each individual RoD. Once users pick a RoD, a *DiffRadar* diagram will be displayed around. The *DiffRadar* diagram shows the detailed statistical variations of the selected fibers.

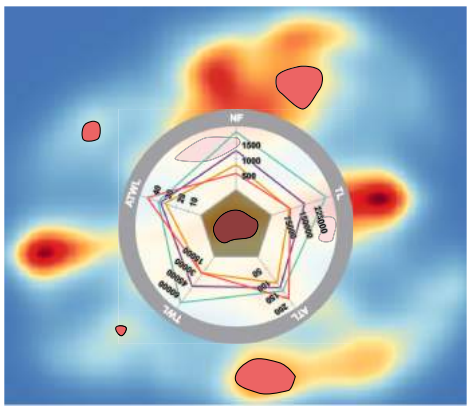

Fig. 5. An example *DiffRadar* diagram. The average density map is displayed at background as a context. RoDs are shown as polygons.

Fig. 5 illustrates the design of our *DiffRadar* diagram. The radial layout is leveraged where each quantitative fiber metric corresponds to one of the equiangular axes. Five widely used fiber metrics are computed for those fibers embedded into the selected RoD: number of fibers (NF), total length (TL), average total length (ATL), total FA weighted length (TWL), and average FA weighted length (ATWL). Please refer to [25] for the computation details. The picked RoD is shown in the center of this diagram. The metrics of a fiber model are connected with polylines. To differentiate fiber models, a categorical color set is used.

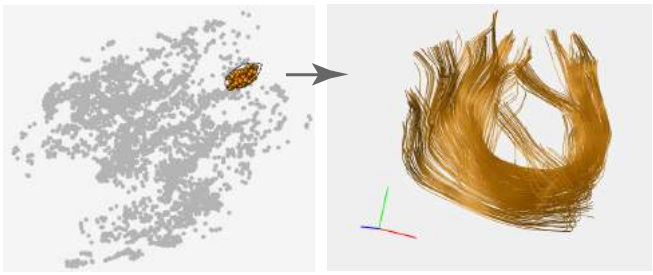

(a) (b)

Fig. 6. Linked exploration: selected fibers in the signature view (a) are immediately rendered as illuminated lines in the 3D fiber view (b).

4. 3D Fiber View

As the axes in signatures do not have intrinsic meanings, linked views and interactions are demanded. Fibers selected from either the signature view or the RoD view are visualized as illuminated lines [45] in the 3D space. Users can easily understand and verify the findings in this view.

V. Implementation

We implemented our approach based on a set of toolkits and libraries. The preprocessing (including data registration, tensor estimation, and fiber tracking) is accomplished using a free software library FSL (http://fsl.fmrib.ox.ac.uk/). Typically several minutes are needed to pre-compute a fiber model on our experimental platform. To generate the signature for each fiber model, the algorithms (Section III.1) are implemented with the standard C++. Computing dissimilarities between fibers are further accelerated with CUDA 5.5. The visualization interface is developed based on Qt 5.1. The rendering of DTI fibers utilized a GPU-accelerated illuminated line algorithm [45].

We have tested our approach in several experiments (more details in Section VI) on a normal PC equipped with an Intel Core 2 Duo 3.0 GHz CPU, 4GB host memory, and an NVIDIA Quadro 4000 video card with 1.5 GB video memory.

VI. Results and Discussions

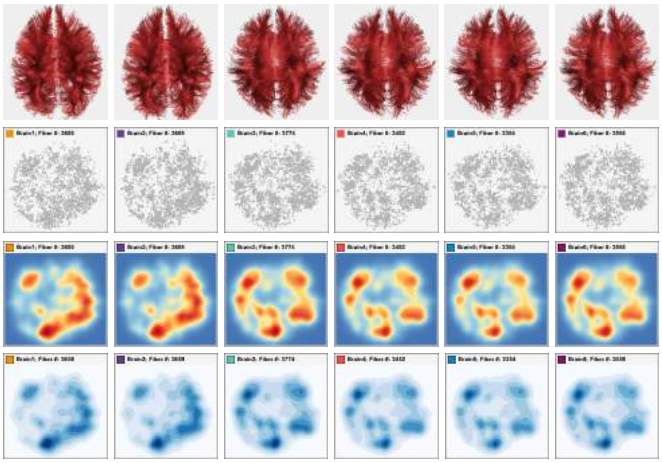

Fig. 7. Comparison of six fiber models generated with different fiber tracking configurations. From left to right the integration step sizes are: 0.75, 0.75, 0.58, 0.58, 0.58, and 0.58. Seeding locations are slightly different among fiber models due to jittering. From top to bottom: the 3D fiber models, the 2D embedding, the continuous density maps, and the contoured density maps.

To evaluate the effectiveness of our approach, we have applied it to two datasets. Table 1 lists the profiles and some major parameters for these datasets including: the data volume resolution (RES), the voxel size (VS), the seeding density (SD), and the culling threshold (CT) that is used in removing short and broken fibers. Moreover, we use 0.25 as the FA threshold and 0.70 as the curvature threshold in processing the fiber models shown in Fig. 7. In order to cover the entire data volume, fibers are generated with a uniform seeding scheme at a high seeding density. Jittering of seeds is exploited to avoid aliasing artifacts. Typically, the generated fibers from the preprocessing component are very dense. The fiber culling operation [43] is then performed to remove the short and broken fibers caused by a partial-volume effect or noise.

Table 1. Profiles of two datasets tested with our approach.

	Atlas Dataset (Section 1)	**Parameter Dataset** (Section 2)
RES	128×128×64	231×172×131
VS (mm)	2.0×2.0×2.0	1.0×1.0×1.0
SD ($seed/mm^3$)	1.0	1.0
CT (mm)	1.0	1.0

1. Fiber Model Characterization

To compare the DTI differences between subjects, we tested our approach on a set of 78 DTI data. Some of the subjects were scanned multiple times in the data. All DWI volumes were scanned based on a GE diffusion tensor imaging protocol with b values (0, 1000) in 72 gradient directions.

The signatures generated with our approach characterize the overall structures and distributional patterns of each fiber model. The scatterplot reveals the similarities among fibers. Similar fibers are positioned close to each other. It is thus natural to perform feature exploration by studying the shape, layout, and distribution in this map. Users can select a region of interest and inspect the selected fibers in the 3D space (see Fig. 6).

Fig. 8 shows the signatures of three healthy subjects **FM1**, **FM2**, and **FM3**, selected from the atlas dataset. Generally, all of them present similar low-dimensional patterns. We can further inspect the detailed differences among them in the RoD view as shown in Fig. 9. From the *DiffRadar* diagram for RoD **R1** in Fig. 9 (a), we find that subject **FM1** has much lower values in terms of quantitative metrics NF, TL, and TWL. However, as shown in Fig. 9 (b) for RoD **R2**, subject **FM1** has slightly higher values in terms of these quantitative metrics compared to subject **FM2** and **FM3**. Anatomical variations mainly contribute to these differences.

From comparing all signature maps of all subjects, we can identify the anatomical structures with a high variance between subjects and those with a low variance. For example, we found that the internal capsule has a high variance between subjects. Along the corpus callosum, the forceps major has a high variance among subjects while forceps minor shows much smaller differences. The difference shown in the signature map can potentially be used to identify the change of the brain anatomy among

a cohort of patients in the longitudinal or cross-sectional studies.

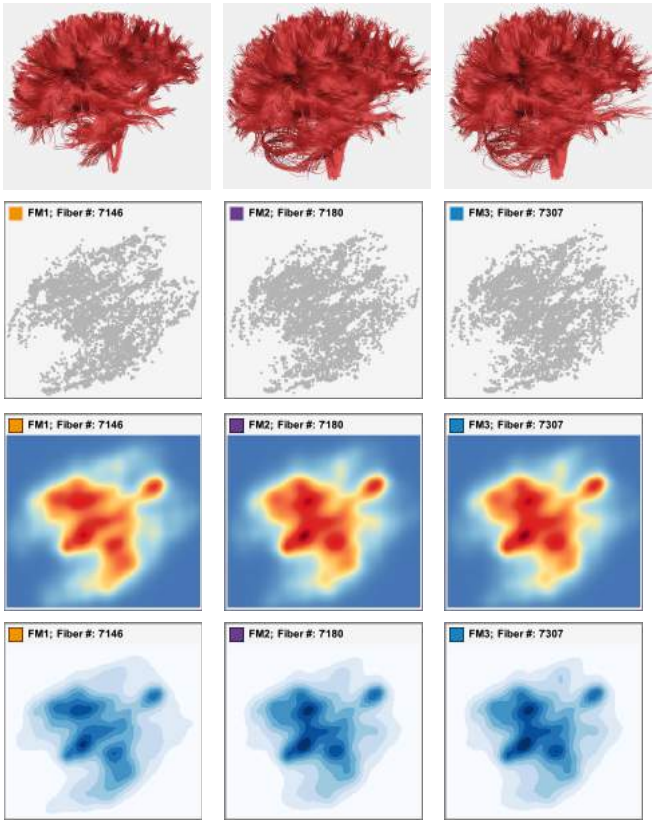

Fig. 8. Results for three fiber models selected from the atlas dataset. From top to bottom: the 3D fiber models, the 2D embedding, the continuous density maps, and the contoured density maps.

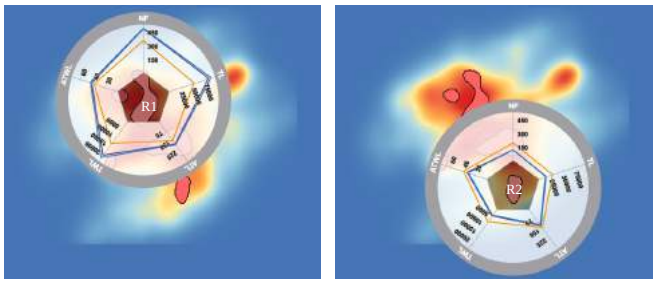

(a) (b)

Fig. 9. The *DiffRadar* diagrams for two RoDs: **R1** and **R2**. The variation of **R1** is higher than that of **R2**.

2. DTI Tracking Parameter Study

The normal human brain DWI volumes used in this experiment were scanned from a SIEMENS 3T MRI scanner with 64 gradient directions and b values (0, 1000).

The pioneering work [5] has studied the influence of stopping criteria on fiber tracking. This experiment intends to investigate whether the integration step size has a great influence on the tracking results. For this purpose, we generate six fiber models with varied integration step size (see Figure 7). All other tracking parameters are the same for each fiber model, except seeding locations caused by jittering.

As demonstrated in the second row of Fig. 7, we can observe that all low-dimensional projection layouts exhibit similar distributions. However, by comparing the generated continuous and contoured density maps in the third and fourth rows, we can see that the first two signatures are quite different from the others. The computed RoDs in Fig. 10 (a) explicitly show the major differences among them. All these observations indicate that the integration step size has a strong effect on the tracking results. That is because the step size determines how long a fiber can move forward and backward in the path tracing process. We also compute the RoDs for the last four signatures (see Fig. 10 (b)). It can be easily verified that fewer RoDs are identified compared with Fig. 10 (a), because there are smaller variations among the last four signatures. These finds also demonstrate that seed jittering does not have much impact on the results after performing the culling operation [43] to remove broken and short fibers.

Our approach provides an intuitive way to discover differences among fiber models. However it lacks the ability to demonstrate how these tracking parameters influence the results.

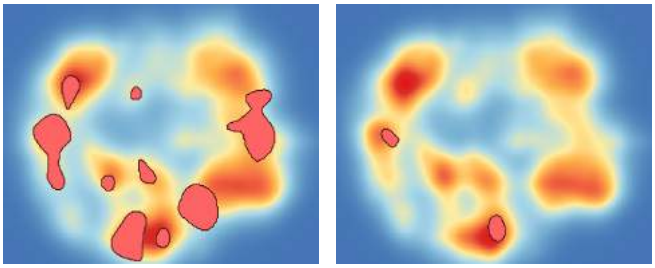

(a) (b)

Fig. 10. The identified RoDs. (a) The RoDs for all six signatures in Fig. 7. (b) The RoDs for the last four signatures in Fig. 7. The same threshold is used to filter out locations of low variations for these two results.

3. Discussions and Future Work Our approach shows promising effectiveness in displaying differences among fiber models. It can be regarded as an adaption of the low-dimensional projection scheme proposed in [16, 38, 17] to multiple datasets comparisons. Our projection scheme uses the same set of *landmark fibers* to build low-dimensional representations for fiber models. The low-dimensional embedding of the *landmark fibers* can be regarded as the backbone of these low-dimensional representations.

We note that projecting a high-dimensional dataset to a 2D plane will inevitably induce errors. The degree of errors depends on the dimensionality of the space, the structure complexity of the dataset, as well as the projection scheme. We will seek to quantify the errors with respect to these factors.

The axes of the low-dimensional projection layout do not have physical meanings. Understanding the projection depends on the user's ability to link locations in the

2D plane to the fibers in the 3D space. Our approach exploits the linked interaction to provide a fast and intuitive correspondence between points in the 2D embedding space and 3D fibers. However, it requires training and exploration time. We plan to enhance the correspondence between the 2D embedding space and the 3D space. One possibility is to label some representative fibers in the 2D embedding space.

Due to the limited human perception capability and screen space, it is challenging to simultaneously compare a large number of signatures in the signature view. The RoD view shows an overview to locate differences among them. However, when diving into the details, visual clutter might be produced in the *DiffRadar* diagram caused by too many overlapped polylines. Clustering and hierarchical exploration are a feasible solution as proven by [22]. This is an avenue for our future work. In addition, effective comparison models will be further studied as well.

The threshold for filtering locations of low variations (see Section III.4) has an effect on the RoD computations. Larger threshold values will produce fewer and smaller RoDs. In our implementation, users can interactively tune this threshold to refine the results.

VII. Conclusion

This paper presents a novel comparative visualization approach for discovering and exploring differences among DTI fiber models. While previous methods compare DTI datasets in either a 3D physical space or a statistical metric space, our approach compares the datasets in a common embedding space. The core is a computation-efficient two-phase projection technique followed by a density estimation process to build the low-dimensional representations of fiber models. Using these low-dimensional representations, regions of significant differences are further explicitly computed. An integrated interface is designed to explore the differences. Experiments on different DTI datasets demonstrate the effectiveness of this approach. Some experts gave positive comments that being able to quickly compare and explore different fibers models with each other is definitely useful.

References

[1] P. J. Basser and C. Pierpaoli. A simplified method to measure the diffusion tensor from seven MR images. *Magnetic Resonance in Medicine*, 39:928–934, 1998.

[2] Patric Hagmann, Lisa Jonasson, Philippe Maeder, Jean-Philippe Thiran, Van J Wedeen, and Reto Meuli. Understanding diffusion mr imaging techniques: From scalar diffusion-weighted imaging to diffusion tensor imaging and beyond 1. *Radiographics*, 26(suppl_1):S205–S223, 2006.

[3] Sinisa Pajevic and Peter J. Basser. Parametric and non-parametric statistical analysis of DT-MRI data. *Journal of Magnetic Resonance*, 163(1):1C14, 2003.

[4] P. J. Basser, S. Pajevic, C. Pierpaoli, J. Duda, and A. Aldroubi. In vivo fiber tractography using DT-MRI data. *Magnetic Resonance in Medicine*, 44:625C632, 2000.

[5] Ralph Brecheisen, Anna Vilanova, Bram Platel, and Bart ter Haar Romeny. Parameter sensitivity visualization for dti fiber tracking. *IEEE Transactions on Visualization and Computer Graphics*, 15(6):1441–1448, 2009.

[6] Brandon Whitcher, David S. Tuch, Jonathan J. Wisco, A. Gregory Sorensen, and Liqun Wang. Using the wild bootstrap to quantify uncertainty in dti. *Human Brain Mapping*, 29(3):346–362, 2007.

[7] Ola Friman and Carl-Fredrik Westin. Uncertainty in white matter fiber tractography. In *Medical Image Computing and Computer-Assisted Intervention–MICCAI 2005*, pages 107–114. Springer, 2005.

[8] Fangxiang Jiao, Jeff M Phillips, Yaniv Gur, and Chris R Johnson. Uncertainty visualization in hardi based on ensembles of odfs. In *IEEE Pacific Visualization Symposium (PacificVis)*, pages 193–200. IEEE, 2012.

[9] Stephen M Smith, Mark Jenkinson, Heidi Johansen-Berg, Daniel Rueckert, Thomas E Nichols, Clare E Mackay, Kate E Watkins, Olga Ciccarelli, M Zaheer Cader, Paul M Matthews, et al. Tract-based spatial statistics: voxelwise analysis of multi-subject diffusion data. *Neuroimage*, 31(4):1487–1505, 2006.

[10] Marco J DaSilva, Song Zhang, Catagay Demiralp, and David H Laidlaw. Visualizing the differences between diffusion tensor volume images. In *Proceedings of the International Society for Magnetic Resonance in Medicine Diffusion MRI Workshop*, 2000.

[11] Stephen Correia, Stephanie Y Lee, Thom Voorn, David F Tate, Robert H Paul, Song Zhang, Stephen P Salloway, Paul F Malloy, and David H Laidlaw. Quantitative tractography metrics of white matter integrity in diffusion-tensor mri. *Neuroimage*, 42(2):568–581, 2008.

[12] Honghui Mei, Haidong Chen, Fangzhou Guo, Wei Chen, Zhang Song, and Guizhen Wang. Visually exploring differences of dti fiber models. In *International Conference on Edutainment*. Springer, 2016. to appear.

[13] F.V. Paulovich, L.G. Nonato, R. Minghim, and H. Levkowitz. Least square projection: A fast high-precision multidimensional projection technique and its application to document mapping. *IEEE Transactions on Visualization and Computer Graphics*, 14(3):564–575, 2008.

[14] Fernando Vieira Paulovich, Danilo Medeiros Eler, Jorge Poco, Charl P Botha, Rosane Minghim, and Luis Gustavo Nonato. Piece wise laplacian-based projection for interactive data exploration and organization. In *Computer Graphics Forum*, volume 30, pages 1091–1100. Wiley Online Library, 2011.

[15] Anushka Anand, Leland Wilkinson, and Tuan Nhon Dang. Visual pattern discovery using random projections. In *Visual Analytics Science and Technology (VAST), 2012 IEEE Conference on*, pages 43–52. IEEE, 2012.

[16] Wei Chen, Zi'ang Ding, Song Zhang, Anna MacKay-Brandt, Stephen Correia, Huamin Qu, John Allen Crow, David F Tate, Zhicheng Yan, and Qunsheng Peng. A novel interface for interactive exploration of dti fibers. *IEEE Transactions on Visualization and Computer Graphics*, 15(6):1433–1440, 2009.

[17] Jorge Poco, Danilo M Eler, Fernando V Paulovich, and Rosane Minghim. Employing 2d projections for fast visual exploration of large fiber tracking data. In *Computer Graphics Forum*, volume 31, pages 1075–1084. Wiley Online Library, 2012.

[18] Michael Gleicher, Danielle Albers, Rick Walker, Ilir Jusufi, Charles D Hansen, and Jonathan C Roberts. Visual comparison for information visualization. *Information Visualization*, 10(4):289–309, 2011.

[19] Hualin Zhou, Min Chen, and Mike F Webster. Comparative evaluation of visualization and experimental results using image comparison metrics. In *Proceedings of the conference on Visualization'02*, pages 315–322. IEEE Computer Society, 2002.

[20] Vivek Verma and Alex Pang. Comparative flow visualization. *IEEE Transactions on Visualization and Computer Graphics*, 10(6):609–624, 2004.

[21] Muhammad Muddassir Malik, Christoph Heinzl, and M Eduard Groeller. Comparative visualization for parameter studies of dataset series. *IEEE Transactions on Visualization and Computer Graphics*, 16(5):829–840, 2010.

[22] Johanna Schmidt, M Eduard Groller, and Stefan Bruckner. Vaico: Visual analysis for image comparison. *IEEE Transactions on Visualization and Computer Graphics*, 19(12):2090–2099, 2013.

[23] Daniela Oelke, Hendrik Strobelt, Christian Rohrdantz, Iryna Gurevych, and Oliver Deussen. Comparative exploration of document collections: a visual analytics approach. In *Computer Graphics Forum*, volume 33, pages 201–210. Wiley Online Library, 2014.

[24] Harald Piringer, Stephan Pajer, Wolfgang Berger, and Heike Teichmann. Comparative visual analysis of 2d function ensembles. In *Computer Graphics Forum*, volume 31, pages 1195–1204. Wiley Online Library, 2012.

[25] Isabelle Corouge, P Thomas Fletcher, Sarang Joshi, Sylvain Gouttard, and Guido Gerig. Fiber tract-oriented statistics for quantitative diffusion tensor mri analysis. *Medical Image Analysis*, 10(5):786–798, 2006.

[26] Casey B Goodlett, P Thomas Fletcher, John H Gilmore, and Guido Gerig. Group statistics of dti fiber bundles using spatial functions of tensor measures. In *Medical Image Computing and Computer-Assisted Intervention–MICCAI 2008*, pages 1068–1075. Springer, 2008.

[27] T Todd Elvins and Ramesh Jain. Web-based volumetric data retrieval. In *Proceedings of the first symposium on Virtual reality modeling language*, pages 7–12. ACM, 1995.

[28] T. Funkhouser, Patrick Min, Michael Kazhdan, Joyce Chen, Alex Halderman, David Dobkin, and David Jacobs. A search engine for 3D models. *ACM Transactions on Graphics*, 22(1):83–105, 2003.

[29] Masaki Hilaga, Yoshihisa Shinagawa, Taku Kohmura, and Tosiyasu L Kunii. Topology matching for fully automatic similarity estimation of 3D shapes. In *Proceedings of the 28th annual conference on Computer graphics and interactive techniques*, pages 203–212. ACM, 2001.

[30] R. Osada, T. Funkhouser, Chazelle, and D. Dobkin. Shape distributions. *ACM Transactions on Graphics*, 21(4):93–101, 2002.

[31] Gevorg Grigoryan and Penny Rheingans. Point-based probabilistic surfaces to show surface uncertainty. *IEEE Transactions on Visualization and Computer Graphics*, 10(5):564–573, 2004.

[32] K. Pöthkow and H.C. Hege. Positional uncertainty of isocontours: Condition analysis and probabilistic measures. *IEEE Transactions on Visualization and Computer Graphics*, 17(10):1393–1406, 2011.

[33] M. Hlawatsch, P. Leube, W. Nowak, and D. Weiskopf. Flow radar glyphs-static visualization of unsteady flow with uncertainty. *IEEE Transactions on Visualization and Computer Graphics*, 17(12):1949–1958, 2011.

[34] K. Potter, J. Kniss, R. Riesenfeld, and C.R. Johnson. Visualizing summary statistics and uncertainty. In *Computer Graphics Forum*, volume 29, pages 823–832, 2010.

[35] Claes Lundstrom, Patric Ljung, Anders Persson, and Anders Ynnerman. Uncertainty visualization in medical volume rendering using probabilistic animation. *IEEE Transactions on Visualization and Computer Graphics*, 13(6):1648–1655, 2007.

[36] SungWon Chung, Ying Lu, and Roland G. Henry. Comparison of bootstrap approaches for estimation of uncertainties of dti parameters. *NeuroImage*, 33(2):531–541, 2006.

[37] Ralph Brecheisen, Bram Platel, Bart M ter Haar Romeny, and Anna Vilanova. Illustrative uncertainty visualization of dti fiber pathways. *The Visual Computer*, 29(4):297–309, 2013.

[38] Radu Jianu, Cagatay Demiralp, and David H Laidlaw. Exploring 3d dti fiber tracts with linked 2d representations. *IEEE Transactions on Visualization and Computer Graphics*, 15(6):1449–1456, 2009.

[39] Paulo Joia, Fernando V Paulovich, Danilo Coimbra, José Alberto Cuminato, and Luis Gustavo Nonato. Local affine multidimensional projection. *IEEE Transactions on Visualization and Computer Graphics*, 17(12):2563–2571, 2011.

[40] Cağatay Demiralp, Radu Jianu, and David H Laidlaw. Exploring brain connectivity with two-dimensional maps. In *New Developments in the Visualization and Processing of Tensor Fields*, pages 187–207. Springer, 2012.

[41] Mark Jenkinson, Peter Bannister, Michael Brady, and Stephen Smith. Improved optimization for the robust and accurate linear registration and motion correction of brain images. *Neuroimage*, 17(2):825–841, 2002.

[42] Vin De Silva and Joshua B Tenenbaum. Sparse multidimensional scaling using landmark points. Technical report, Stanford University, 2004.

[43] Song Zhang, Stephen Correia, and David H Laidlaw. Identifying white-matter fiber bundles in dti data using an automated proximity-based fiber-clustering method. *IEEE Transactions on Visualization and Computer Graphics*, 14(5):1044–1053, 2008.

[44] B.W. Silverman. *Density estimation for statistics and data analysis*. Chapman & Hall/CRC, 1986.

[45] Ovidio Mallo, Ronald Peikert, Christian Sigg, and Filip Sadlo. Illuminated lines revisited. In *Proceedings of IEEE Visualization*, pages 19–26. IEEE, 2005.

MEI Honghui (corresponding author) was born in Nanjing. He received the B.S. degree and now be a Ph.D. candidate in Zhejiang University, China. His research interests include visualization and visual analytics. (Email: meihonghui.zju@gmail.com)

CHEN Haidong received the B-S degree from Northeast Normal University, China, the masters degree and the Ph.D. degree from Zhejiang University, China. His research interests include uncertainty visualization and highdimensional data visualization. (Email: chenhd925@gmail.com)

GUO Fangzhou was born in ... . He received the Ph.D. degree in electronic engineering from Cambridge University, UK. He is a professor of ... . His research interests include ... and ... . (Email: guofz1234@gmail.com)

ZHANG Fan was born in ... . He received the Ph.D. degree in electronic engineering from Cambridge University, UK. He is a professor of ... . His research interests include ... and ... . (Email: fanzhang@cad.zju.edu.cn)

SONG Zhang received the BS degree in computer science from Nankai University in 1996 and the PhD degree in computer science from Brown University in 2006. He is an associate professor in the Department of Computer Science and Engineering, Mississippi State University. His research interests include scientific visualization, data analysis, medical imaging, and computer graphics. He is a senior member of the IEEE. (Email: szhang@cse.msstate.edu)

WANG Guizhen received BE degree in Engineering at College of Computer Science and Technology and the Ph.D. degree in Zhejiang University. Her research interests include Visual Analytics and Human Computer Interaction. (Email: wguizhen@gmail.com)

CHEN Wei received the PhD degree in Fraunhofer Institute for Graphics, Darmstadt, Germany, in July 2002. He is a professor in State Key Lab of CAD & CG, Zhejiang University, China. From July 2006 to September 2008, he was a visiting scholar at Purdue University. His current research interests include visualization and visual analytics. He is a member of the IEEE. (Email: chenwei@cad.zju.edu.cn)